

A practical approach to extract symplectic transfer maps numerically for arbitrary magnetic elements

Yongjun Li

Brookhaven National Laboratory, Upton, NY-11973

Xiaobiao Huang

SLAC National Accelerator Laboratory, Menlo Park, CA-94025

(Dated: September 30, 2018)

We introduce a practical approach to extract the symplectic transfer maps for arbitrary magnetic beam-line elements. Beam motion in particle accelerators depends on linear and nonlinear magnetic fields of the beam-line elements. These elements are usually modeled as magnetic multipoles with constant field strengths in the longitudinal direction (i.e., hard-edge model) in accelerator design and modeling codes. For magnets with complicated structures such as insertion devices or fields with significant longitudinal variation effects, the simplified models may not be sufficient to characterize beam dynamics behaviors accurately. A numerical approach has been developed to extract symplectic transfer maps from particle trajectory tracking simulation that uses magnetic field data provided by three-dimensional magnetic field modeling codes or experimental measurements. The extracted transfer maps can be used in linear optics design and nonlinear dynamics optimization to achieve more realistic results.

PACS numbers: 41.85.-p

I. INTRODUCTION

The designing and modeling of modern accelerators heavily rely on computer codes such as MAD [1], Elegant [2], Accelerator Toolbox [3]. In these codes, simplified magnet models are widely used to calculate the transfer maps, which characterize the transportation of charged particle through the magnets. Typically magnets are described as multipole fields about the design trajectory without longitudinal variation. Thus symplectic transfer maps can be easily obtained for such so-called hard-edge models. However, the field strengths of real magnets always have longitudinal variations, at least in the transition regions at both ends (i.e., fringe fields). Although the magnetic field data in three-dimensional (3D) space can usually be calculated with electro-magnetic field solvers, it is rather difficult to extract the transfer maps from the discrete field data directly.

Transfer maps characterizing the realistic fields are preferable in magnetic element modeling. First, the fringe field effects can be incorporated into the models. The consequences of the fringe fields are particularly important for small rings with large acceptance and for beams with large emittances as pointed out by Berz in Ref [4]. It could also be critical for large rings with many magnets, such as the proposed ultimate storage rings (USRs) [5], which typically consists of many closely-packed strong magnets. In addition, the cross-talk of the fringe fields of adjacent magnets could cause significant differences between the real machines and the simplified lattice models in such a scenario. Second, special magnets, such as insertion devices or combined-function dipoles with straight geometry [6], can be accurately integrated into the lattice models. By studying the discrepancies between the realistic fields and the simplified

magnet models, one can identify if each individual model is sufficiently accurate from the view of linear and nonlinear beam dynamics.

It is strongly desirable that transfer maps are symplectic because symplecticity is essential in the study of long-term beam stability. Lie map, which ensures the symplecticity property of a Hamiltonian system, was introduced by Dragt [7] into beam dynamics and is now widely used in the accelerator community. The purpose of this paper is to present a general and practical approach to extract the Lie transfer map of an arbitrary magnet by symplectifying the Taylor maps that are obtained by fitting direct particle trajectory simulation data. An alternative method by surface field fitting to extract maps for straight-axis magnetic elements can be found in Ref. [8].

Our approach aims at constructing accurate lattice models by improving the accuracy of individual magnet elements and potentially including the cross-talk effects of adjacent magnets in the models. Accurate lattice models not only make nonlinear dynamics optimization results based on the models more reliable, but also make machine commissioning easier since the initial set-points of the magnets would be more accurate.

The paper is organized as follow: Section II reviews some basic concepts of transfer maps for a Hamiltonian system and briefly introduces the method established by Dragt and Finn [9] to extract a Lie map from a set of Taylor map series. In Section III we discuss the procedure of map extraction step by step. Three detailed examples are given in Section IV as demonstrations of its application. The paper concludes with a summary in Section V.

II. TRANSFER MAPS

A. Basic concepts

We consider a dynamical system that is composed of a charged particle moving through the field of a magnet. Ignoring radiation, the transportation of the particle from the entrance face to the exit face of the magnet can be represented by a transfer map in the six-dimensional phase space of the canonical coordinates of the particle

$$X = [x, p_x, y, p_y, z, \delta]^T. \quad (1)$$

Here superscript T indicates vector transpose. As in most accelerator physics literature [10], we use the path-length s as the free variable. Therefore (x, p_x) , (y, p_y) and $(z = s - ct, \delta = \frac{P - P_0}{P_0})$ are three pairs of canonical coordinates, which satisfy the Hamilton equations

$$\dot{q}_i = \frac{\partial H}{\partial p_i}, \quad \dot{p}_i = -\frac{\partial H}{\partial q_i}, \quad (2)$$

where $q_i = x, y, z$ and $p_i = p_x, p_y, \delta$ for $i = 1, 2, 3$, respectively. The dots mean derivatives respective to the free variable s and H is the Hamiltonian of the system. The Lie transfer map for an infinitesimal slice of the magnetic field can be expressed as [7]

$$\begin{aligned} M(s \rightarrow s + \Delta s) &= e^{-H(s)\Delta s} = e^{:G:} \\ &= \left[1 + :G: + \frac{:G:^2}{2!} + \dots \right], \end{aligned} \quad (3)$$

where $G = -H(s)\Delta s$ is referred to as the Lie map generator and Δs is the length of the field slice. Following Dragt [7], the Lie operator in Eq. (3) is defined to signify the Poisson bracket, i.e.,

$$:f:g = [f, g] = \sum_{i=1}^3 \frac{\partial f}{\partial q_i} \frac{\partial g}{\partial p_i} - \frac{\partial f}{\partial p_i} \frac{\partial g}{\partial q_i} \quad (4)$$

for operator $:f:$ acting on function g . The powers of an operator are defined as

$$\begin{aligned} (:f:)^2 g &= f : (f : g) = [f, [f, g]], \\ (:f:)^3 g &= [f, [f, [f, g]]], \dots, \text{ etc.} \end{aligned} \quad (5)$$

In general, the Lie map generators of beam-line elements can be expressed as polynomials of the canonical coordinates

$$G = \sum_{abcdef} C_{abcdef} x^a p_x^b y^c p_y^d z^e \delta^f. \quad (6)$$

For example, $G = -\frac{(p_x^2 + p_y^2)L}{2}$ represents a drift space with length L . It is convenient to express G as [11]

$$G = \sum_{abcdef} C_{abcdef} |abcdef\rangle \quad (7)$$

where C_{abcdef} is the coefficient of the monomial term

$$|abcdef\rangle = x^a p_x^b y^c p_y^d z^e \delta^f. \quad (8)$$

The transfer map of a beam-line composed of a series of magnet elements can be obtained by joining the transfer maps of the individual magnets in sequence [11]

$$M = e^{:f_1:} e^{:f_2:} \dots e^{:f_n:}, \quad (9)$$

where $e^{:f_i:}$ is the transfer map of the i -th element. By means of Lie algebra manipulations, such as similarity transformation and Baker-Campbell-Hausdorff (BCH) theorem [7, 11], one can concatenate them into a single Lie map, which is known as the *one-turn-map* in accelerator physics literature if the beam-line is a closed loop.

Obviously, in order to obtain an accurate one-turn map to be used in simulation and analysis, the transfer maps of the individual magnets need to characterize the realistic fields precisely.

B. Taylor map and Lie map

The Taylor map approach plays an important role in the design of charged-particle transport systems, such as linear accelerators, synchrotron storage rings and spectrometers. The canonical coordinates of a charged particle at the magnet exit are expressed as an expanded multivariate Taylor power series of the coordinates at its entrance [12]

$$X_{i,1} = \sum_{j=1}^6 R_{ij} X_{j,0} + \sum_{j,k=1, j \leq k}^6 T_{ijk} X_{j,0} X_{k,0} + \dots, \quad (10)$$

where R and T are the 1st- and 2nd-order transfer map coefficients, $X_{j,0}$ and $X_{j,1}$ are the j -th canonical coordinate at the entrance and the exit, respectively.

Taylor maps can be very accurate in describing single pass trajectories. But they are usually not symplectic. Therefore, they are not suitable for the study of long-term stability in periodical structures, such as storage rings. When simulating the trajectory of a relativistic particle under the Lorentz force by solving the ordinary differential equations (ODE), the tracking result can be made very close to a symplectic transformation by choosing small step sizes and tight convergence criteria with non-symplectic integrators. Symplectic ODE integrators [13] are also available. But they are usually implicit integrators and are time-consuming. Dragt and Finn have proved that [9], given a symplectic Taylor map in the form of Eq. (10), there exists an infinite series of homogeneous multivariate polynomial Lie generators of ascending orders, $G^{(2)}$, $G^{(3)}$, etc., such that the map Eq. (10) can be written in the form

$$X_{i,1} = \left[e^{:G^{(2):} : e^{:G^{(3):} : \dots} \right] X \Big|_{X=X_{i,0}}, \quad (11)$$

where $G^{(i)}$, $i \geq 2$ is an i -th order homogeneous polynomial. This method is known as the Dragt-Finn factorization.

The factorization is realized by calculating the homogeneous generators order by order. First the 2nd-order generator can be derived from the linear matrix (equivalent to the map $e^{G^{(2)}}$):

$$R_{ij} = \frac{\partial X_{i,1}}{\partial X_{j,0}}. \quad (12)$$

To go to higher orders, the inverse map $e^{-G^{(2)}}$ is applied to the Taylor map Eq. (10) in order to obtain the residual map $e^{-G^{(2)}}: X_1 - X_0 = X_r^{(2)} + O(3)$ (here $O(3)$ indicates third or higher order terms) which should have no linear terms left over. The quadratic terms in the residual map, $X_{r,i}^{(2)}$, $i = 1, 2, \dots, 6$, are the partial derivatives of an exact differential. The 3rd order homogeneous generator $G^{(3)}$ is therefore given by a path integral [9]

$$G^{(3)} = - \int^X \sum_{ij} X_{r,i}^{(2)} S_{ij} dX'_j, \quad (13)$$

where S is the 6×6 asymmetric symplecticity matrix with $S_{ij} = [X_i, X_j] =: X_i: X_j$. The same process can be repeated to higher orders or when no higher order generator exists. It can be verified that the path integral for the n^{th} ($n \geq 3$) generator is given by

$$G^{(n)} = -\frac{1}{n} \sum_{ij} X_{r,i}^{(n-1)} S_{ij} X_j, \quad (14)$$

where $X_{r,i}^{(n-1)}$ is the $(n-1)^{\text{th}}$ order polynomial terms in the corresponding residual map $e^{-G^{(n-1)}}: \dots e^{-G^{(2)}}: X_1 - X_0$.

If we can obtain near-symplectic Taylor maps by fitting simulated multi-particle trajectories, it is straightforward to convert them to Lie maps via Dragt-Finn factorization. Taylor maps to arbitrary orders can also be obtained with the technique of differential algebra (DA) [14]. To do so, the magnetic field must be given in explicit functions of coordinates. In most cases, it is difficult and time-consuming to fit analytic functions to the discrete data on a 3D grid.

III. PROCEDURE OF EXTRACTING TRANSFER MAP

For a given magnet, the procedure of extracting the Lie transfer map through trajectory simulation is summarized in the following six steps:

1. *Obtaining the magnetic field data on a 3D grid.* The size of the grid on which the three field components are given should be fine enough for 3D data interpolation during the trajectory simulation. If the grid is too sparse, the interpolated magnetic

field might not be able to satisfy the Maxwell equations.

2. *Determining the reference orbit.* For straight line elements, such as quadrupoles, wigglers, etc., the reference orbit is a straight line passing through the magnet center. For curved magnets such as dipoles, the reference orbits may need to be numerically determined by finding a nominal particle trajectory that passes through the field under certain conditions. More details on curved reference orbit will be discussed in the second example in Section IV. The coordinates of all particles at both the entrance and exit faces need to be converted relative to the local reference orbit.
3. *Implementing multi-particle trajectory simulation.* The effects of the magnetic field to beam motion are sampled by tracking multiple particles through the field. The initial phase space coordinates of the particles need to be populated evenly in the area of interest. For example, if we are studying the dynamic aperture of a storage ring, the area in phase space should be larger than the expected dynamic aperture at the magnet location. The number of coordinate values on each phase space direction should be sufficient in order to resolve the potential nonlinear effects to a certain order. In practice, multiple particle trajectory simulation is the most time consuming in this procedure (e.g., it takes 20 hrs. for the 2-m magnet with a 1 mm step size in the second example in section IV with serial computation.). However, this simulation only needs to be done once and the difficulty can be easily overcome by carrying out the simulation in parallel, if necessary.
4. *Fitting simulation results to Taylor maps.* The Taylor map for particle coordinates from the entrance face to the exit face can be obtained by fitting the multi-particle tracking results with the least square minimization approach. The number of Taylor map coefficients can be calculated by

$$\sum_{k=1}^{\Omega} \frac{(n+k-1)!}{(n-1)k} \times n, \quad (15)$$

where n is the number of variables and Ω the order of the Taylor map. In order to ensure the minimization problem to be over-determined, the number of particles must be larger than the number of the coefficients. We can increase the particle number step by step until the Taylor map begins to converge within a tolerance. The order of the Taylor maps depends on the highest order of Lie generators user want to extract. For example, if one wants to generate up to the 4th order Lie generators, the corresponding Taylor maps must be calculated to the 3rd order, or even higher.

5. *Factorizing the Taylor map into a Lie map.* The procedure of deriving a Lie map from Taylor maps is discussed in detail in Ref. [9] and has been briefly recounted in Section II B. It can be regarded as an automatic process of “repairing” the symplecticity property of the dynamical system. For each order of the factorization, after the inverse map is applied, the residual errors of this order should be exactly zeros because the corresponding generator is an exact path integral for a symplectic map. By dropping off the residual errors, the slight error of symplecticity due to, e.g. the numerical errors in 3D data interpolation, the implementation of non-symplectic integrators in solving the ODEs, etc., are rounded off. On the other hand, the residual errors serve as an indication of the symplectic quality of the Taylor map obtained from fitting the trajectory simulation data. The factorization process can stop at a certain order, or when no higher order generators exist.

6. *Validating the Lie map by comparing to the simulation data.* The accuracy of the Lie map can be checked by evaluating the transportation of individual particles using Eqs. (3) and (11), and comparing the results with trajectory tracking results. The comparison indicates the quality of the Lie map, and may also suggests whether one needs to push the factorization to higher orders in order to get a precise transfer map.

The Lie map obtained with the above procedure serves as an accurate and concise description of the element. It can be used for non-symplectic particle tracking with Eqs. (11) and (3) while truncating at the desired order. It is also possible to implement symplectic tracking with the map. One symplectic tracking method is achieved by splitting the exponential map of polynomials into a series of exponential maps of monomials with the BCH formulas [11]. Each monomial exponential map can be evaluated symplectically.

In the next section, three applications are given for the purpose of demonstration of the method.

IV. APPLICATIONS

A. Fringe field of a quadrupole

Studies of magnet fringe field effects can be found in many accelerator literature [4, 15–17]. The purpose of this example is to benchmark our approach against the well-established COSY-Infinity code [18], which provides an accurate soft fringe model for quadrupoles based on the differential algebra (DA) technique [14].

Consider a quadrupole with a soft fringe field at its exit as illustrated in FIG. 1. The nominal field gradient is $\frac{\partial B_y}{\partial x} = -18$ T/m and the effective length $L_{\text{eff}} = 0.1$ m.

The fringe field fall-off profile is described by the Enge function with six parameters [18]

$$F(s) = \frac{1}{1 + \exp\left(\sum_{i=1}^6 a_i \frac{(s-s_0)^{i-1}}{D}\right)}, \quad (16)$$

where $D = 0.05$ m is the full aperture and $s_0 = 0.1$ m is the effective field boundary. We calculate the quadrupole field on a 3D grid based on Eq. (16) with the default Enge coefficients in COSY, $a_i = 0.296471, 4.533219, -2.270982, 1.068627, -0.036391, 0.022261$ for $i = 1$ to 6.

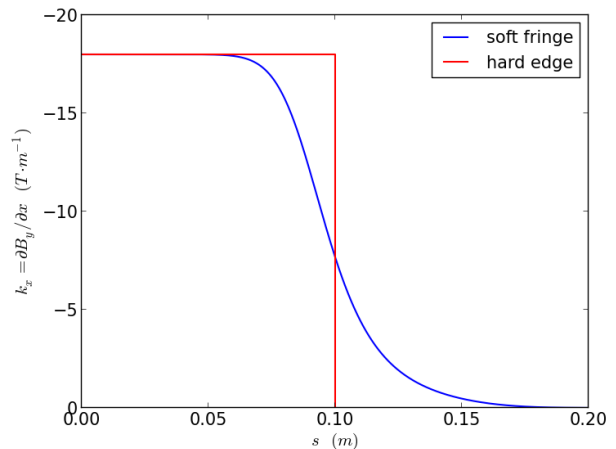


FIG. 1. A soft fringe field profile described by Enge function

Here we want to obtain the transfer map for a 3 GeV electron beam by following the procedure summarized in section III. The reference orbit is the straight line passing through the quadrupole center. Multiple particles with different initial coordinates are tracked through the magnet by using the Runge-Kutta ODE integration method to solve the equations of motion under the Lorentz force. The longitudinal free coordinate s must cover the fringe field region for the trajectory simulation. All coordinates at both the entrance and the exit are recorded, from which the Taylor transfer map is extracted. Finally the Lie transfer map is factorized from the Taylor map. The comparison of the nonvanishing 4th order homogeneous polynomial coefficients between the two approaches (FIG. 2) shows that they agree with each other very well.

The obtained transfer map has been validated by evaluating Eqs. (11) and (3) for each simulated particle. By using the first three generators $G^{(2-4)}$ and truncating the exponential map Eq. (3) at the 5th-order, the standard deviations (RMS) of the discrepancy between the direct trajectory simulation and the map transportation are found to be less than 1×10^{-7} m or rad for the phase space coordinates.

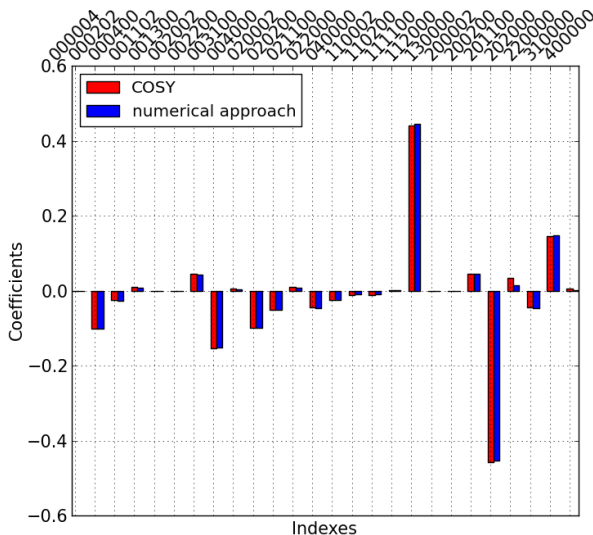


FIG. 2. Comparison of the nonvanishing 4th-order homogeneous polynomial coefficients between COSY and the numerical approach.

B. Combined-function dipole with a Cartesian gradient

The dipole magnets of SPEAR3 and a few other storage rings are combined-function magnets built with a straight geometry [6, 19]. Therefore, the magnetic field seen by a particle and its curvature of trajectory vary along the path inside the magnet (see FIG. 3), in addition to variations in the fringe regions. A direct trajectory tracking has been used to study the linear and nonlinear effects of this type of magnets [20]. But the method is non-symplectic and computationally very slow and is hence not suitable for beam dynamics optimization.

The magnetic field for the SPEAR3 dipole in this study is based on the analytic field model in Ref. [20] which was derived from magnetic field measurements on the mid-plane.

First, the reference orbit is obtained by launching a particle on the mid-plane with the nominal energy (3 GeV) and the nominal entrance angle (half of the nominal deflection angle) and varying its launching position until a symmetric trajectory is found. The particle trajectories need to start and end in field-free locations. The reference trajectory is shown in FIG. 3. Multiple particle trajectories about the reference trajectory are simulated with tracking. The dynamic aperture at the location of the dipole is less than 1 cm for both transverse planes because of the small horizontal beta function ($\beta_x < 2$ m) at the location and small vertical physical apertures at the insertion devices. Therefore the input position coordinates for trajectory simulation are populated evenly within a 1 cm \times 1 cm box in the x - y plane.

In accelerator lattice design, it is preferable to model a magnet compactly with hard edges at an appropriate

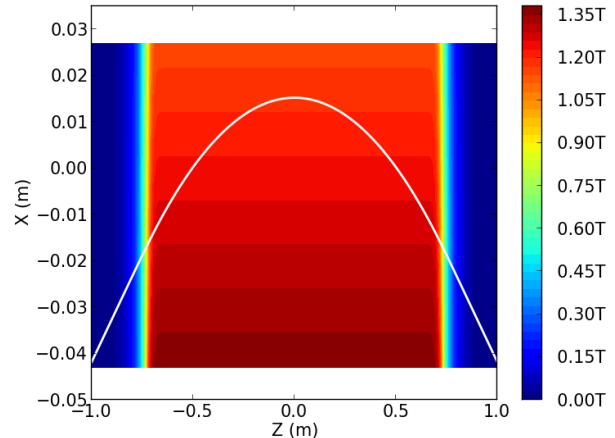


FIG. 3. Contour of the vertical field component of a standard SPEAR3 dipole in the mid-plane. The white line is the reference orbit obtained by simulation.

effective length. This can be realized by adding two virtual negative length drifts on both sides, as illustrated in FIG. 4. Starting from the entrance of the hard-edge model, the particles first drift backward to the field-free region (step 1). Then the particles are tracked through the magnetic field region (step 2). Finally at the exit side the particles again drift backward from the field-free edge to the hard-edge boundary (step 3). Because numerical tracking is done on the Cartesian coordinates, coordinate transformations are needed between the usual Frenet-Serret coordinate system and the Cartesian coordinate system at the hard edge boundaries of both ends.

With the tracking results from the above setup and the procedure described in section III, we calculated the transfer map for an equivalent hard-edge model for the dipole that includes the fringe field effects. This map can be incorporated into a lattice model for beam dynamics analysis. The linear transfer matrix for the SPEAR3 dipole is listed in Table I, and the first few monomial coefficients in generators $G^{(3-4)}$ are listed in descending order in Table III. The RMS values of discrepancy between the trajectory simulation and the map transportation are around 2.5×10^{-5} m or rad if the three generators $G^{(2-4)}$ are used for evaluation. The discrepancy will be further reduced to around 1.1×10^{-5} m or rad if the generator $G^{(5)}$ is implemented.

A usual hard-edge sector dipole model can be derived from the magnetic field profile of the SPEAR3 dipole. The effective length is 1.50694 m, the bending angle is $\pi/17$ and the focusing strength is $K_1 = -0.3117031$ m⁻². The difference between this simplified model and the Lie map obtained numerically can be accounted for with a virtual thin-lens corrector element attached at the end of the sector dipole model. The linear transfer matrix for this corrector is shown in Table II, which represents linear errors of the best sector dipole model. Incorporating

corrector elements like this into the lattice model would improve model accuracy.

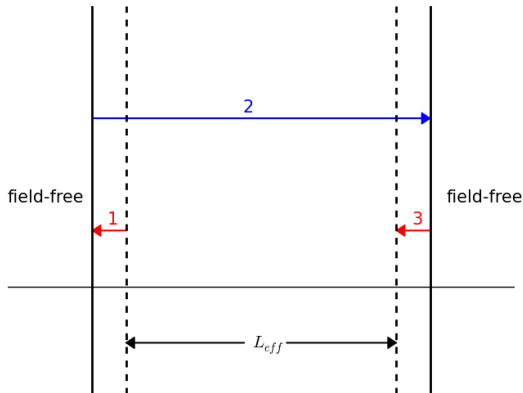


FIG. 4. Illustration of the procedure to obtain the transfer map for an equivalent hard-edge model by adding two virtual negative drifts (the step 1 and 3 shown as red arrows) at the ends.

TABLE I. 6D Linear transfer matrix for a standard SPEAR3 dipole (in SI units, same below)

| | | | | | |
|----------|----------|----------|---------|---|----------|
| 1.37520 | 1.68361 | 0 | 0 | 0 | 0.14747 |
| 0.52933 | 1.37521 | 0 | 0 | 0 | 0.20804 |
| 0 | 0 | 0.65202 | 1.33404 | 0 | 0 |
| 0 | 0 | -0.43092 | 0.65202 | 0 | 0 |
| -0.20804 | -0.14747 | 0 | 0 | 1 | -0.00905 |
| 0 | 0 | 0 | 0 | 0 | 1 |

TABLE II. A correction transfer matrix at the exit end of the sector dipole model to account for the difference between such a model and the Lie map for a standard SPEAR3 dipole

| | | | | | |
|----------|---------|----------|----------|---|----------|
| 0.99898 | 0.00246 | 0 | 0 | 0 | -0.00013 |
| -0.00089 | 1.00102 | 0 | 0 | 0 | 0.00003 |
| 0 | 0 | 0.99947 | -0.00092 | 0 | 0 |
| 0 | 0 | -0.00023 | 1.00053 | 0 | 0 |
| -0.00003 | 0.00013 | 0 | 0 | 1 | -0.00015 |
| 0 | 0 | 0 | 0 | 0 | 1 |

C. Insertion device integration

Insertion devices (ID), such as wigglers and undulators, are the main x-ray sources in modern storage ring light sources. Usually their first and second field integrals

TABLE III. Part of the 3rd- and 4th-order generator coefficients for the SPEAR3 dipole

| a | b | c | d | e | f | Coefficient |
|-----|---|---|---|---|---|-------------|
| 0 | 2 | 0 | 0 | 0 | 1 | 1.13814 |
| 0 | 0 | 0 | 2 | 0 | 1 | 0.75041 |
| 1 | 1 | 0 | 0 | 0 | 1 | -0.49203 |
| 1 | 2 | 0 | 0 | 0 | 0 | -0.38990 |
| 0 | 1 | 1 | 1 | 0 | 0 | 0.37658 |
| ... | | | | | | |
| 0 | 2 | 0 | 0 | 0 | 2 | -1.45884 |
| 1 | 3 | 0 | 0 | 0 | 0 | 1.13290 |
| 2 | 2 | 0 | 0 | 0 | 0 | -0.91574 |
| 0 | 0 | 0 | 2 | 0 | 2 | -0.74524 |
| 0 | 4 | 0 | 0 | 0 | 0 | -0.67212 |
| ... | | | | | | |

are required to be zeros so that they can be regarded as straight beam-line elements, although the real reference orbits inside the magnet bodies actually wiggle, or spiral around a straight line.

Several symplectic integrators [21–23] are available for particle tracking through IDs. But in some cases, it is desirable to have explicit transfer maps. For example, by integrating IDs into the one-turn map of the storage ring, their contributions to the nonlinear resonance driving terms (NRDT) can be calculated quantitatively.

We use an elliptical polarized undulator (EPU) of the NSLS-II NEXT project [24] as an example to illustrate the application of our method to IDs. The magnetic field for the vertical polarized mode of this device is calculated using the code RADIA [25]. The first few main generator coefficients of $G^{(4)}$ for one period of the device are listed in descending order in Table IV. As expected, the EPU has some very weak sextupole-like components in $G^{(3)}$ (not listed in the table). But the dominant contributions are from the vertical octupole-like components in $G^{(4)}$. These terms contribute directly to the 2nd order driving terms, and eventually affect the storage ring dynamic aperture. Because the coefficients given in Table IV are for only one period and an EPU typically have tens of periods, the device could have a significant impact on the nonlinear dynamics of the storage ring. Therefore it is necessary to incorporate IDs into the storage ring lattice optimization.

It is interesting to compare the Lie transfer map we obtained against the direct trajectory simulation and the kick-map [21] calculated by RADIA [25]. We chose a set of particles with different initial horizontal offsets within the $[-2, 2]$ cm range and a fixed vertical offset at $y = 2$ mm and transported them through one period of the EPU with the Runge-Kutta integrator, the Lie transfer map and the kick-map integrator, respectively.

TABLE IV. Part of the 4th-order generator coefficients for one of the NSLS-II EPUs

| a | b | c | d | e | f | Coefficient |
|-----|---|---|---|---|---|-------------|
| 0 | 0 | 4 | 0 | 0 | 0 | -1.60204 |
| 0 | 0 | 1 | 3 | 0 | 0 | 1.07844 |
| 1 | 1 | 2 | 0 | 0 | 0 | 0.10163 |
| 2 | 0 | 2 | 0 | 0 | 0 | 0.06378 |
| 2 | 0 | 1 | 1 | 0 | 0 | 0.05501 |
| 1 | 3 | 0 | 0 | 0 | 0 | -0.04480 |
| ... | | | | | | |

Using the results of the Runge-Kutta integrator as the reference, the discrepancies of the other two integrators with respect to the reference at different initial horizontal coordinates are shown in FIG. 5. Although both the kick-map integrator and Lie generator can achieve results with an error of $\Delta x'_{max} < 1.0 \mu\text{rad}$, the Lie transfer map has better performance in terms of absolute errors and the smoothness of the error curve. It is not straightforward to obtain the Lie map from the 3D field data. But it is worth doing, not only because the Lie map can generate better results in tracking, but also because it can be directly used in calculating the contribution to the resonance driving terms.

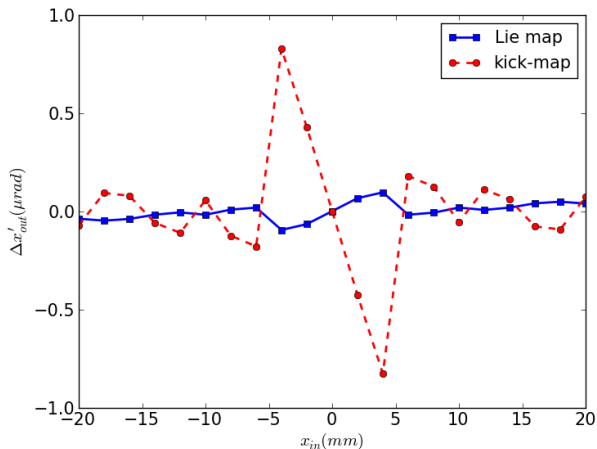


FIG. 5. Discrepancy of the horizontal exit angles between the Lie generators (transfer map) and the kick-map generator after passing through one period of the EPU at different initial coordinates. The Runge-Kutta integrator's result is used as the reference. The vertical offset is fixed at 2 mm.

To calculate the contributions to the 2nd-order driving terms from the extracted Lie transfer map, we need to expand the Lie generator $G^{(4)}$ to a polynomial in the betatron oscillation resonance basis [11]

$$h_{x,y}^{\pm} = \sqrt{2J_{x,y}} e^{\pm i\phi_{x,y}} = (\bar{x}, \bar{y}) \mp i\bar{p}_{x,y}, \quad (17)$$

where $J_{x,y}$ and $\phi_{x,y}$ are action-angle variables, \bar{x}, \bar{y} and $\bar{p}_{x,y}$ normalized coordinates which are related with the

Courant-Snyder parameters $\alpha_{x,y}, \beta_{x,y}$ at the location of the ID through

$$\begin{bmatrix} \bar{x} \\ \bar{p}_x \end{bmatrix} = \begin{bmatrix} \frac{1}{\sqrt{\beta_x}} & 0 \\ \frac{\alpha_x}{\sqrt{\beta_x}} & \sqrt{\beta_x} \end{bmatrix} \begin{bmatrix} x \\ p_x \end{bmatrix}, \quad (18)$$

and likewise for the y -plane. The new generator polynomial in the resonance basis can be expressed as

$$G^{(4)} = \sum_{\substack{i,j,k,l,m=0 \\ i+j+k+l+m=4}} C_{ijkl,m} |ijkl, m\rangle, \quad (19)$$

where the monomial signifies

$$|ijkl, m\rangle = (h_x^+)^i (h_x^-)^j (h_y^+)^k (h_y^-)^l \delta^m. \quad (20)$$

Here only five power indexes appear in Eqs. (19) and (20) because the $z = s - ct$ coordinate has no dynamic effect in an ID. It is well-known that $C_{1111,0}$, $C_{2200,0}$ and $C_{0022,0}$ are related to the three first order tune-shift-with-amplitude coefficients, which are important in dynamic aperture optimization.

V. CONCLUSION

We have introduced a general method to extract a symplectic transfer map for an arbitrary beam-line element from direct trajectory simulation through its magnetic field. A Taylor map is first obtained by fitting the multi-particle trajectory tracking data, which is then turned into a Lie map with the Dragt-Finn factorization [9]. The method is demonstrated with applications to three practical examples, including the fringe field effect of quadrupoles, dynamic effects of a straight-geometry combined-function dipole and an insertion device.

The Lie map obtained with our method can be used in lattice models to study linear and nonlinear beam dynamics effects of various beam-line elements that may have been left out in existing codes, such as combined-function dipoles on straight-geometry that are used on a few storage ring light sources. Another potential application is the study of the cross-talk effect between adjacent beam-line elements. This could be especially important for future ultimate storage rings. The proposed USR lattice designs are similar to that of the MAX-IV [26] storage ring in which many small magnets are closely packed. By applying our numerical approach to a sequence of magnets to extract a combined symplectic transfer map, we may directly study the beam dynamics with the cross-talk effects included, or separate the cross-talking effects from each individual magnet by introducing correction maps in between.

ACKNOWLEDGMENTS

We thank Prof. Dragt and his student Dr. Mitchell for many useful discussions, Prof. Berz and his student Dr.

H. Zhang for help in using COSY-Infinity, and Dr. Kitegi for providing the NSLS-II EPU field data. We are also grateful to J. Safranek and S. Krinsky for their pertinent comments on an earlier version of the manuscript. Work at Brookhaven National Laboratory was supported by

the U.S. Department of Energy, Office of Science, Office of Basic Energy Sciences, under Contract No. DE-AC02-98CH10886. Work at SLAC National Accelerator Laboratory was supported by the U.S. Department of Energy, Office of Science, Office of Basic Energy Sciences, under Contract No. DE-AC02-76SF00515.

-
- [1] H. Grote and F. Schmidt, (2003), CERN-AB-2003-024-ABP.
- [2] M. Borland, (2000), Advanced Photon Source LS-287.
- [3] A. Terebilo, (2001), SLAC-PUB-8732.
- [4] M. Berz, B. Erdelyi, and K. Makino, Nucl.Instrum.Meth. **A472**, 533 (2000).
- [5] E. S. Reich, Nature **501**, 148 (2013).
- [6] J. Corbett, D. Dell’Orco, Y. Nosochkov, and J. Tanabe, (1999), SLAC-PUB-8234.
- [7] A. Dragt, AIP Conf.Proc. **87**, 147 (1982).
- [8] C. Mitchell and A. Dragt, Phys.Rev.ST Accel.Beams **13**, 064001 (2010).
- [9] A. Dragt and J. Finn, J.Math.Phys. **17**, 2215 (1976).
- [10] S. Y. Lee, *Accelerator physics* (World Scientific, 1999).
- [11] A. Chao, (2002), SLAC-PUB-9574.
- [12] K. Brown, (1968), SLAC-R-075, SLAC-75.
- [13] J. Sanz-Serna, BIT **28**, 877 (1988).
- [14] M. Berz, Part.Accel. **24**, 109 (1989).
- [15] H. A. Enge, Rev.Sci.Instrum. **35**, 278 (1964).
- [16] E. Forest and J. Milutinovic, Nucl.Instrum.Meth. **A269**, 474 (1988).
- [17] F. Zimmermann, (2000), CERN-SL-2000-012-AP, CERN-NUFACT-NOTE-22.
- [18] M. Berz and K. Makino, (2006), MSUHEP-060804.
- [19] M. Yoon, J. Corbett, M. Cornacchia, J. Tanabe, and A. Terebilo, Nucl.Instrum.Meth. **A523**, 9 (2004).
- [20] X. Huang, J. Safranek, and D. Dell’Orco, Proceedings of IPAC 2010 , 4626 (2010).
- [21] P. Elleaume, EPAC’92 , 661 (1992).
- [22] Y. Wu, E. Forest, and D. Robin, Phys.Rev. **E68**, 046502 (2003).
- [23] J. Bahrtdt and G. Wustefeld, Phys.Rev.ST Accel.Beams **14**, 040703 (2011).
- [24] Brookhaven National Labortary, “NSLS-II NEXT Project,” (2013).
- [25] O. Chubar, P. Elleaume, and J. Chavanne, J.Synchrotron Radiat. **5**, 481 (1998).
- [26] S. Leemann, A. Andersson, M. Eriksson, L.-J. Lindgren, E. Wallen, *et al.*, Phys.Rev.ST Accel.Beams **12**, 120701 (2009).